Journal of Zhejiang University-SCIENCE A (Applied Physics & Engineering) *2024 25(7):573-585*
www.jzus.zju.edu.cn; www.springer.com/journal/11582
E-mail: jzus_a@zju.edu.cn

Research Article
https://doi.org/10.1631/jzus.A2300251

Time-synchronous-averaging-spectrum based on super-resolution analysis and application in bearing fault signal identification

Zengle REN[1], Yuan WANG[2], Huiyue TANG[3], Xin'an CHEN[4], Wei FENG[1,5,6,*]

[1]*Guangdong Provincial Key Laboratory of Construction Robotics and Intelligent Construction, Shenzhen Institute of Advanced Technology, Chinese Academy of Sciences, Shenzhen 518055, China*
[2]*Shenzhen EBORAIL Technology Co., Ltd., Shenzhen 518038, China*
[3]*National Supercomputing Center in Shenzhen, Shenzhen 518055, China*
[4]*State Key Lab of Rail Traffic Control and Safety, Beijing Jiaotong University, Beijing 100044, China*
[5]*University of Chinese Academy of Sciences, Beijing 100190, China*
[6]*Shenzhen University of Advanced Technology, Shenzhen 518107, China*

Abstract: Time-synchronous-averaging (TSA) is based on the idea of denoising by averaging, and it extracts the periodic components of a quasiperiodic signal and keeps the extracted waveform undistorted. This paper studies the mathematical properties of TSA, where three propositions are given to reveal the nature of TSA. This paper also proposes a TSA-spectrum based on super-resolution analysis and it decomposes a signal without using any base function. In contrast to discrete Fourier transform spectrum (DFT-spectrum), which is a spectrum in frequency domain, TSA-spectrum is a period-based spectrum, which can present more details of the cross effects between different periodic components of a quasiperiodic signal. Finally, a case study is carried out using bearing fault analysis to illustrate the performance of TSA-spectrum, where the rotation speed fluctuation of the shaft is estimated, which is about 0.12 ms difference. The extracted fault signals are presented and some insights are provided. We believe that this paper can provide new motivation for TSA-spectrum to be widely used in applications involving quasiperiodic signal processing (QSP).

Key words: Time-synchronous-averaging (TSA); Spectrum; Quasiperiodic signal processing (QSP); Super-resolution analysis; Bearing fault detection

1 Introduction

This paper presents an innovative approach in the field of quasiperiodic signal processing (QSP) by introducing the time-synchronous-averaging-spectrum (TSA-spectrum) based on super-resolution analysis. QSP is essential in various applications, from medical science to engineering, where the extraction of periodic components from signals is crucial. While Fourier transform (FT) has traditionally been used to transform signals from time to frequency domains, we explore the concept of period as an independent parameter in the analysis of quasiperiodic signals. We provide an overview of the significance of QSP, the limitations of traditional frequency-based methods, and the unique characteristics of period-based analysis. In the subsequent section, we delve into the background of our research to offer a comprehensive understanding of the context and motivation behind the proposed TSA-spectrum.

1.1 Background

Using FT, we can transform a signal from a time domain into a frequency domain. As is known, a period is the reciprocal of a frequency. A spectrum in a frequency domain naturally corresponds to a spectrum in a period domain. More specifically, both the terms 'period' and 'frequency' mentioned herein are parameters of a sine or cosine function. However, intrinsically, the concept of 'period' should be independent from the existence of a sine or cosine function. When we try to liberate 'period' from FT, the liberated

✉ Wei FENG, wei.feng@siat.ac.cn
Wei FENG, https://orcid.org/0000-0002-9845-999X

Received May 9, 2023; Revision accepted Dec. 5, 2023;
Crosschecked June 16, 2024

period is not the reciprocal of the frequency of any base functions, such as sine, cosine, and wavelet functions. Without a specific base function, the period is a more general concept describing a periodic signal.

Mathematically, a signal $y(t)$ is a periodic signal if there exists a $T \in \mathbb{R}^+$ satisfying $y(t) = y(t+T)$ for all $t \in \mathbb{R}$. The parameter T denotes the period of $y(t)$.

We name a nonperiodic signal with hidden periodic components as a quasiperiodic signal, which can be described as

$$\hat{y}(t) = y(t) + g(t),$$

where $y(t)$ is the periodic component and $g(t)$ is a nonperiodic term.

In real applications, either $y(t)$ or $g(t)$ may contain the information of interest. QSP refers to signal processing techniques able to identify or extract the information we want, while at the same time eliminating or suppressing other information. The exact purpose of QSP depends on the needs of the actual application.

QSP covers a wide range of application scenarios, from medical science and climate analysis to general usage in engineering. For medical science, QSP can be applied to electrocardiography (ECG) to monitor heart conditions (Lin et al., 2008; Martens et al., 2018; Wang et al., 2023), and QSP techniques can be used with electroencephalograms (EEG) to reveal the activity of the human brain (Thakor and Tong, 2004; Chaumon et al., 2015; Mannan et al., 2018; Nagwanshi and Potnis, 2023). For applications in engineering, we can apply QSP to analyze the vibration signals of rotating machinery, such as bearings (Randall and Antoni, 2011; Wang et al., 2014; Smith and Randall, 2015; Yao et al., 2022) and gears (Sun et al., 2018; Touret et al., 2018; Wang et al., 2018b; Tan et al., 2021), for fault diagnosis and early warning. This can be of crucial importance for the operational safety of high-speed trains (Hong et al., 2014; Chen et al., 2019; Peng et al., 2019; Gabrić et al., 2021), wind turbines (Qiao and Lu, 2015; Salameh et al., 2018; Wang et al., 2019), and engines (Wang et al., 2013; Delvecchio et al., 2018; Ma et al., 2019).

Currently, there are many signal processing techniques pertaining to QSP methods, such as FT (Gothwal et al., 2011; Lee et al., 2014; Talhaoui et al., 2014; Sugavanam et al., 2019; Ma and Tao, 2021; Thibault et al., 2023), wavelet transforms (Chen et al., 2016; Wang et al., 2018a; Gupta et al., 2019; Tian et al., 2023), and many other filtering methods (Roth et al., 2017; Li YF et al., 2018; Zhang et al., 2019; Bommert et al., 2020). Almost all these techniques share a common point that relates to a spectral description in the frequency domain. In this paper, we call a signal processing technique a frequency-based method if it analyzes a signal in a frequency domain based on a base function, such as a sine, cosine, or wavelet function. In contrast, we name a technique a period-based method if it analyzes a signal in the period domain. It should be noted that TSA can be taken as a typical period-based method for signal processing (McFadden, 1987). TSA is not new, but it is classic and effective. Hereafter, this paper is mainly focused on TSA and we introduce the TSA-spectrum based on super-resolution analysis from the aspect of the period spectrum. A brief review of TSA is presented in Section 1.2.

1.2 Brief review of time-synchronous-averaging (TSA)

TSA is a technique with a long history and there is much related literature. It is based on the idea of denoising by averaging and it does not rely on any base function. It is widely used in condition evaluation of rotating equipment, such as bearings (Mishra et al., 2016; Yao et al., 2022) and gearboxes (Combet and Gelman, 2007; Halim et al., 2008; Ahamed et al., 2014; Bravo-Imaz et al., 2017; Camerini et al., 2019; Zhang and Hu, 2019; Tan et al., 2021). TSA can extract periodic components from a signal and keep the extracted waveform undistorted. The performance of TSA in processing signals, such as vibration and noise, of a device with rotating structures has been well studied.

TSA is ergodic and its denoise property can be described as follows. Non-synchronous noise is reduced by the reciprocal of the square root of the number of revolutions (McFadden, 1987). The only parameter of TSA is the length of the synchronous signal which, in most publications dealing with bearings or gearboxes, is related to the revolution of the rotating shaft. Usually, a tachometer, or speed sensor, is necessary to provide a reference value of the length of the synchronous signal (McFadden and Toozhy, 2000; Mishra et al., 2016; Schmidt et al., 2021). However, since it is hard to determine accurately the rate of revolution, researchers

have proposed solutions to estimate its possible value by some data-driven approaches (Fong et al., 2020; Syed and Muralidharan, 2022; Zhao et al., 2022).

There are many improvements and applications of TSA, which combine TSA with other signal processing techniques such as wavelet transform (WT) or empirical mode decomposition (EMD), including impact synchronous time averaging (ISTA) (Rahman et al., 2011), time-synchronous moving average (TSMA) (Zhang and Hu, 2019), multiple-pulse individually rescaled-time synchronous averaging (MIR-TSA) (Ahamed et al., 2014), TSA with windows (de Smidt, 2010; Pitarresi et al., 2020; Gao et al., 2023), and TSA algorithm in frequency domain (McFadden and Toozhy, 2000; Mishra et al., 2016; Roy et al., 2016; Sim et al., 2022). It should be noted that the performance of TSA can be enhanced by resampling before averaging, mostly by interpolation (McFadden, 1989), which is taken as super-resolution analysis of TSA.

1.3 Contribution of this paper

In this paper, we propose the TSA-spectrum for visualizing possible periodic components of a signal in the period domain. While TSA is concise and simple, the mathematical properties concerning performance on quasiperiodic signals are intricate. The essential mathematical characteristics of TSA are presented in three propositions, backed by the congruence theory in number theory. Our work in this paper introduces several significant advances on the existing literature:

(1) Theoretical framework and enhanced visualization

We establish the theoretical framework of TSA with vital definitions and propositions. The TSA-spectrum is introduced to shed light on the periodic components concealed within a signal. In terms of visualization, our method offers an intuitive representation that promotes quicker and more precise fault diagnosis. Furthermore, super-resolution analysis is brought in to augment the efficacy of the TSA-spectrum (discussed in electronic supplementary materials (ESM)).

(2) Comparison with DFT

The relationship and divergence between the TSA-spectrum and the discrete Fourier transform spectrum (DFT-spectrum) are meticulously explored. In a theoretical context, TSA emerges as a pivotal complement to DFT, especially in the long-period (low-frequency) domain. This distinction highlights the precision of the TSA method in capturing and representing cyclic variations, which sets it apart from conventional techniques (elaborated in Section 2).

(3) Empirical validation with bearing-fault analysis

We undertake a comprehensive case study focusing on bearing-fault analysis. By deploying the TSA-spectrum on a public dataset of bearing vibration readings, we effectively extract fault signals associated with distinct bearing defects. Such insights are novel, with no similar revelations recorded in the bearing-fault diagnosis sphere. Importantly, our results underline the commendable performance of the TSA-spectrum on QSP, reinforcing its adaptability and versatility in identifying a range of bearing-faults. This, combined with its computational efficiency, paves the way for its potential in real-time applications (detailed in Section 3).

In conclusion, our efforts in this paper not only introduce a novel approach in the form of the TSA-spectrum but also validate its strengths and advantages over existing methods in the literature. We trust that these contributions address the current gaps and foster further research and exploration in the domain.

2 Relationship and difference between TSA-spectrum and DFT-spectrum

This section discusses the relationship and difference between the DFT and TSA. DFT is mainly based on the concept that a finite-energy signal can be described as a combination of a series of sine or cosine functions. In contrast, TSA is derived from the essential characteristics of a periodic signal and is quite different from signal processing techniques based on signal decomposition using sine or cosine functions. A comparison between TSA and DFT is illustrated in Fig. 1.

Taking the rectangular function $S(t;T_0)$ with the period T_0 as an example, as shown in Fig. 1a, in the time domain, we have

$$S(t;T_0)=\begin{cases}1, & t\in\left[0,\ \dfrac{T_0}{2}\right)+kT_0,\\ -1, & t\in\left[\dfrac{T_0}{2},\ T_0\right)+kT_0,\end{cases}$$

where $k\in\mathbb{Z}$ and $S(t;T_0)=S(t+T_0;T_0)$. If T_0 is a period, kT_0 is also the period of $S(t;T_0)$.

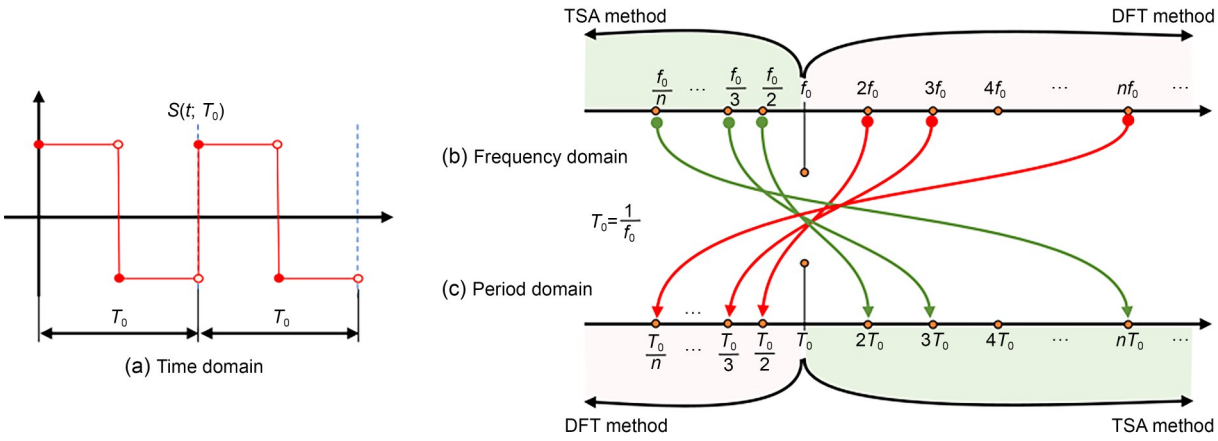

Fig. 1 Comparison between TSA and DFT in the frequency and period domains

If we apply DFT to a sequence sampled from $S(t;T_0)$, we can only obtain information at the angular frequencies $f>f_0=1/T_0$ in the frequency domain. For example, we can observe peaks in the DFT-spectrum at kf_0 and $k\in\mathbb{N}^+$, but we know nothing for frequencies with $f<f_0$. In contrast, when we apply TSA to a sequence sampled from $S(t;T_0)$, we can obtain the information in the period range of $T\geqslant T_0$ in the period domain. For example, we can observe peaks in the TSA-spectrum at kT_0 and $k\in\mathbb{N}^+$. Furthermore, an interesting finding is that for some specific cases, we can also obtain information for the period range $T<T_0$, or more exactly, for those T values satisfying $(T,T_0)=d>1$, which can be explained by Proposition 1 given in the ESM. In conclusion, DFT is more powerful in dealing with high-frequency (short-period) components but is helpless for low-frequency (long-period) components where TSA makes up for the weakness of DFT.

It should be noted that TSA can be shown to be powerful when comparing performances of TSA and DFT in two cases: (1) a rectangular signal with only one period, 100, denoted as $y_1(t)$, and (2) a signal combining two rectangular functions with periods 100 and 150, denoted as $y_2(t)$.

$$y_1(t)=S(t;100)+e(t),$$
$$y_2(t)=0.5\cdot S(t;100)+0.5\cdot S(t;150)+e(t).$$

For both cases, a noise term $e(t)$ is added. It is white noise with a zero mean and a standard deviation of 1. For both cases, we sample 2^{16} (=65536) data points with the sampling frequency $F_s=1$ Hz. Then two discrete sequences, Y_1 and Y_2 from $y_1(t)$ and $y_2(t)$ respectively, are obtained. Lastly, TSA and DFT are applied to both Y_1 and Y_2. The results of the TSA-spectrum and the DFT-spectrum are presented in Fig. 2. Here, L/T represents the ratio of the length of the original data piece (L) to the rotation period (T) of the bearing.

It can be seen in Fig. 2a that there are obvious peaks for operation cycles $T=100k$ and $k\in\mathbb{N}^+$. Furthermore, we can also observe small peaks at $T=20k$ and $k\in\mathbb{N}^+$. In contrast, in Fig. 2b, we can observe peaks at $f=(2k-1)/100$ and $k\in\mathbb{N}^+$ in the frequency domain. However, the DFT-spectrum provides little information for $f<0.01$. In the result presented in Fig. 2c, the major peaks of the TSA-spectrum are located at 100, 150, 200, 300, ⋯, which shows the interaction between these two rectangular functions. It should be noted that there is a newly generated period of 300, which is the least common multiple of 100 and 150. Moreover, we can find small peaks for $T<100$ in the period domain. In contrast, we can observe peaks at $f=(2k-1)/100$ and $k\in\mathbb{N}^+$ and at $f=(2k-1)/150$ and $k\in\mathbb{N}^+$ in the frequency domain in Fig. 2d, but no information is provided for $f<1/150$.

Fig. 3 provides a crucial demonstration of the practical advantages of TSA over DFT in scenarios involving signals with low signal-to-noise ratios (SNRs). The physical interpretation of Fig. 3 is as follows:

In Fig. 3a, we initially encounter a noise-free signal. Taking the sequence sampled from $y_2(t)$ as an example, it can be found that the maximal magnitude of Y_2 without noise is 1, which is equal to the standard deviation of the white noise. However, as noise

is introduced in Fig. 3b, the original waveform becomes nearly indistinguishable due to the low SNR.

TSA comes to the forefront as a powerful solution to this challenge. Fig. 3c showcases the TSA vector when the operation cycle is set to 100. This specific choice effectively extracts the underlying periodic components, thus revealing the original signal, even in the presence of substantial noise. Fig. 3d unveils another facet of TSA. Here, the operation cycle is configured at 150, resulting in the extraction of a single period of $0.5 \cdot S(t; 150)$. Importantly, the result in Fig. 3c is not merely a singular period of $0.5 \cdot S(t; 100)$. Instead, it represents a blend of one period of $0.5 \cdot S(t; 100)$ and the TSA outcome of $0.5 \cdot S(t; 150)$, utilizing an

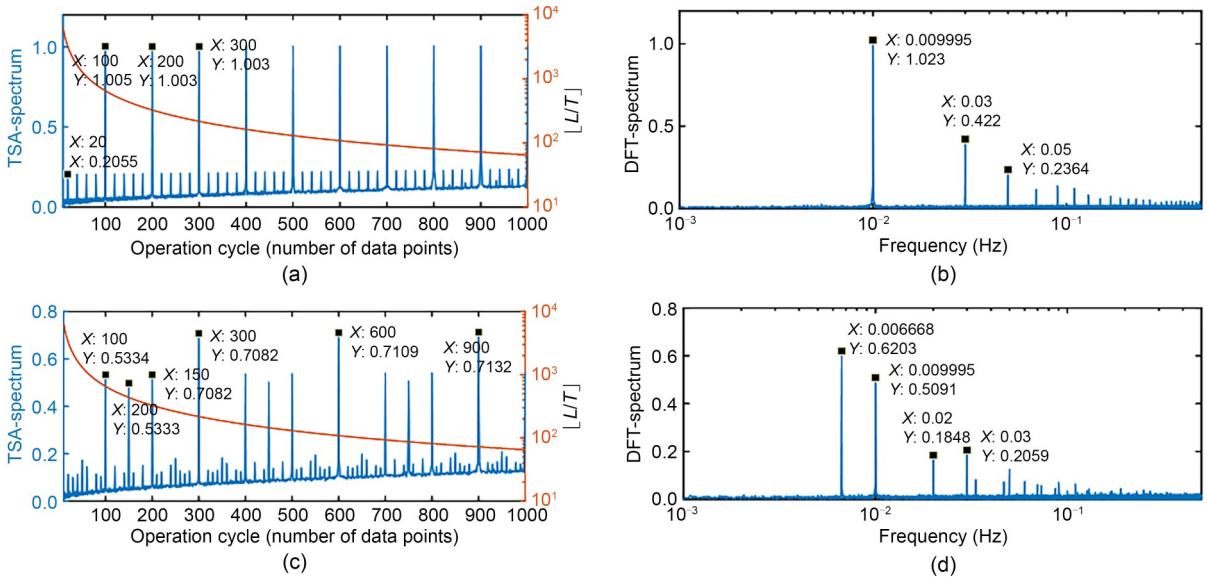

Fig. 2 Comparison between the TSA-spectrum and DFT-spectrum: (a) TSA-spectrum of Y_1; (b) DFT-spectrum of Y_1; (c) TSA-spectrum of Y_2; (d) DFT-spectrum of Y_2

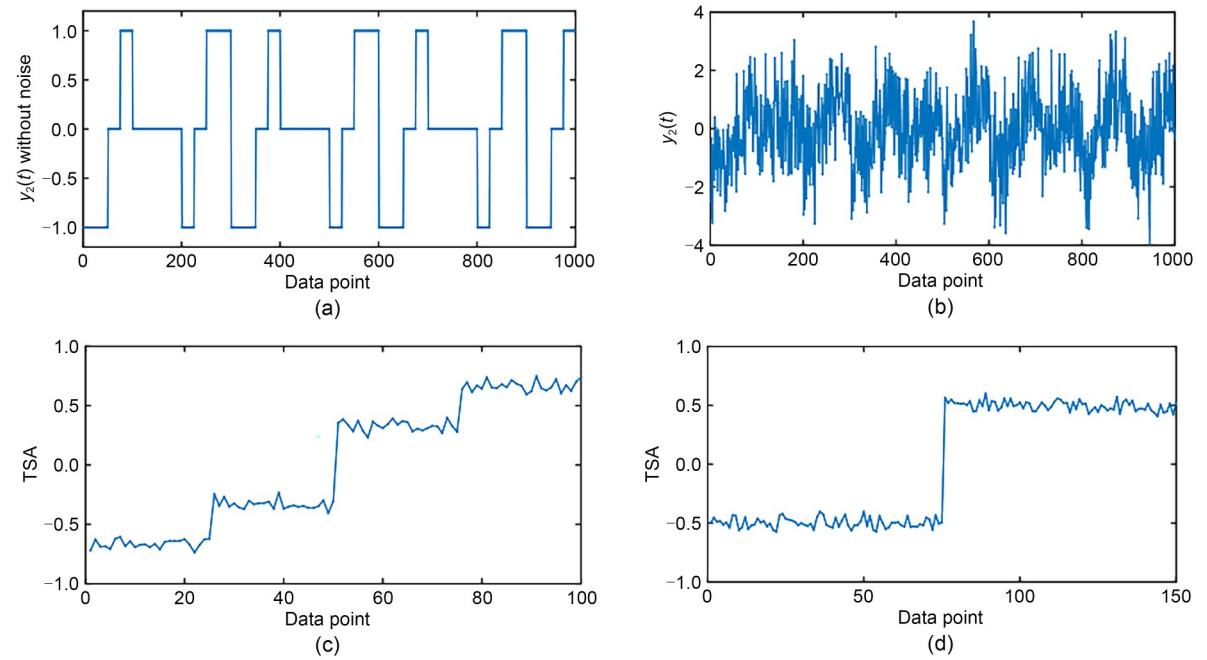

Fig. 3 Signal extraction performance of TSA: (a) Y_2 without noise; (b) Y_2 with noise; (c) TSA vector with the operation cycle set to 100; (d) TSA vector with the operation cycle set to 150

operation cycle of 150. This phenomenon, known as the period aliasing phenomenon (PAP), occurs when a signal encompasses two periodic components with periods T_1 and T_2 satisfying $(T_1, T_2)=d>1$.

In summary, Fig. 3 effectively illustrates how TSA triumphs in extracting vital periodic components from noisy signals. This visual representation underscores TSA's prowess in addressing the challenges posed by low SNR scenarios. Furthermore, it highlights the occurrence of the PAP as a critical aspect of TSA's signal processing capability, ultimately enhancing signal extraction, even when confronted with challenging noise levels.

3 Application to the bearing test dataset

To illustrate the performance of TSA, this section presents an application of TSA for bearing-fault diagnosis. The vibration of a rotating bearing provides a stable quasiperiodic signal which can be a good example of the advantages of TSA. The dataset used in this section is the widely used bearing test dataset published by Case Western Reserve University (CWRU, 2019).

3.1 Problem description

Bearings are one of the greatest inventions of mankind. As a type of typical rotating machinery, bearings are widely used in all kinds of vehicles, trains, wind turbines, engines, etc. (Teng et al., 2017; Li YF et al., 2018; Lin et al., 2018). Therefore, it is of great importance to develop accurate and robust bearing-fault diagnosis techniques to keep machines safe and reliable. In this section, we take a typical rolling bearing 6205-2RS JEM SKF as an example. The structure of Bearing 6205 consists of an inner raceway, an outer raceway, and a cage train with multiple rolling elements, as illustrated in Fig. 4.

In practice, the vibration of a rotating bearing is a typical quasiperiodic signal. A perfect bearing helps the inner shaft rotate freely and smoothly. Unfortunately, it can fail due to mechanical damage, crack, wear damage, etc. When a failure occurs, a series of high-level short pulses in acceleration can be observed, owing to the ball passing over the defect and causing the bearing to vibrate abnormally. For example, as illustrated in Fig. 5, there is a defect on the inner raceway. The vibration of the bearing will contain a short-period signal caused by the ball hitting the defect between points B and A. The period of the fault signal is related to the diameters $2R$ and $2r$ and to the angular speed of the shaft.

To address the performance of TSA, we transfer data from the CWRU dataset (CWRU, 2019) to the TSA-spectrum through a multi-step process. Information on these four data samples is presented in Table 1. Each data sample is collected in an independent test process. Initially, we collect vibration data from the CWRU dataset, encompassing signals from various bearing conditions and machinery types. Subsequently, we apply data preprocessing techniques such as cleaning, noise reduction, and resampling to ensure data uniformity. The pivotal step involves employing TSA to align periodic components within the data, followed by the calculation of the TSA-spectrum. From the TSA-spectrum, we extract pertinent features that capture the distinctive characteristics of periodic components. These extracted features serve as valuable inputs for

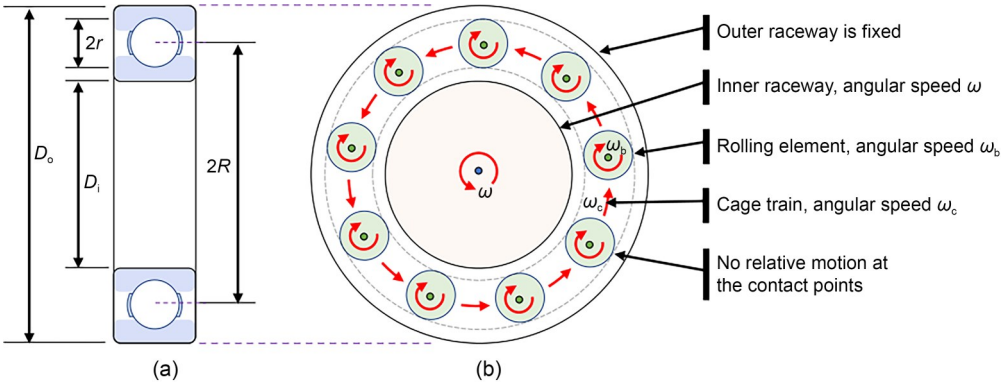

Fig. 4 Illustration of the structure of Bearing 6205-2RS JEM SKF. $2R$=39.03 mm, $2r$=7.94 mm, D_o=52.00 mm, and D_i=25.00 mm. There are nine rolling elements

machine learning models employed in bearing condition classification and fault detection. The computational overhead of this data transfer process varies depending on the dataset size and the available computational resources. To enhance efficiency, we explore optimization strategies, including parallel computing and judicious feature selection. This comprehensive data transformation process is an integral part of our research, facilitating the accurate and effective identification of bearing-faults for predictive maintenance and machinery reliability improvement.

Additionally, since there is no relative motion at the contact points between the rolling elements and the inner or outer raceway, the relationship between the angular speeds ω and ω_c is given as $\omega_c/\omega=(R-r)/(2R)$. For Bearing 6205, we have $\omega_c/\omega \approx 0.4$, indicating that for every 2.5 cycles of the inner race, the cage train moves exactly 1 cycle.

3.2 Results of TSA

3.2.1 Major cycle analysis using TSA-spectrum

First, we apply TSA to four different types of bearing signals and calculate their TSA-spectra, as presented in Fig. 6. It should be noted that the File IDs in Table 1 correspond to the sub-figures in Fig. 6. The TSA-spectrum can reveal the cycles hidden inside a measured sequence. Note that since the length of the original data piece and the rotation velocity of the bearing are different from each other, the maximal value of the sample number, namely, the maximum of $\lfloor L/T \rfloor$ in the right axis of each subfigure, varies

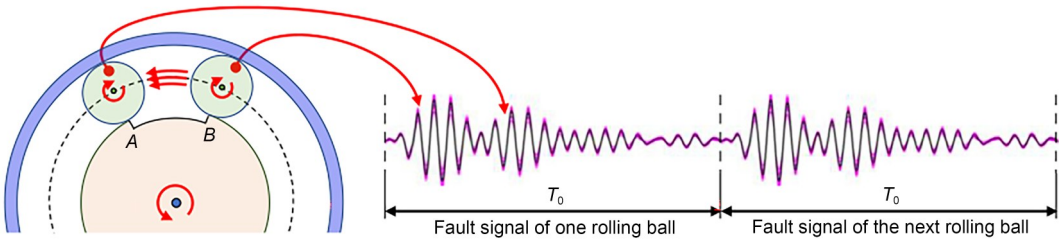

Fig. 5 Hidden periods in the vibration signal of a rotating bearing with defects

Table 1 Four data samples from the seeded fault test data published by CWRU (2019)

File ID	Sample number	Fault type	Operating condition	Fault size
1	100	Normal	1725 r/min, 0 kW	0.1778 mm
2	122	Ball failure (BF)	1796 r/min, 0 kW	
3	109	Inner raceway failure (IRF)	1796 r/min, 0 kW	
4	135	Outer raceway failure centered to load (ORF_CE)	1797 r/min, 0 kW	

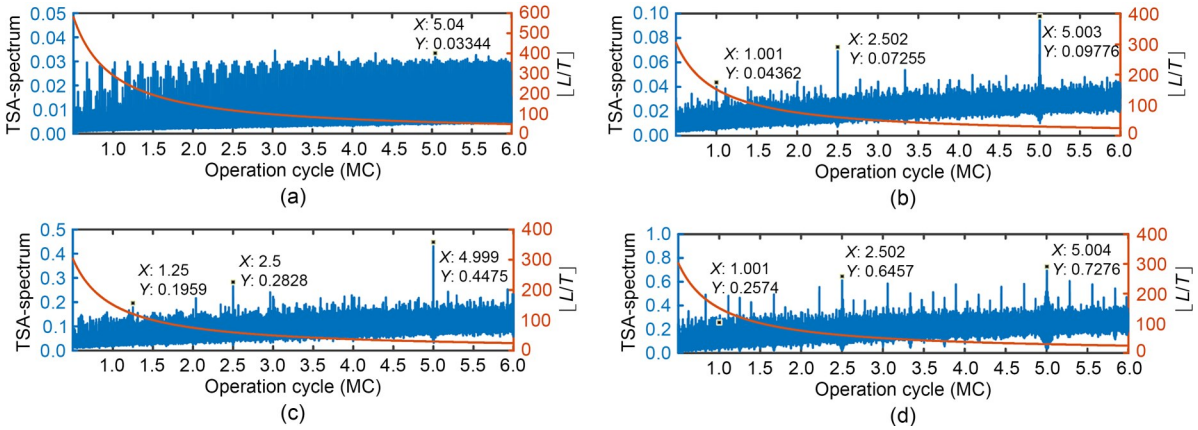

Fig. 6 Comparison between the TSA-spectra of the four different signal types when a 48000×3 sampling frequency is applied: (a–d) Files 1–4. The unit MC means the number of data points for one cycle of the rotation shaft

for different measured data. By comparing the four TSA-spectra in Fig. 6, the following conclusions can be drawn:

1. In Fig. 6a, all peaks show similar values, and the values of the TSA-spectrum are smaller than those in Figs. 6b and 6d. This suggests that the bearing condition represented in Fig. 6a is relatively more stable, with less variance in its signal.

2. Except Fig. 6a, all other TSA-spectra show obvious peaks approximately at 2.5 and 5.0 MC. The unit MC means the number of data points for one cycle of the rotation shaft. These peaks indicate prominent cycle repetitions at these intervals, hinting at specific bearing conditions that recur with each rotation.

3. In Fig. 6b, associated with a bearing experiencing ball failure, a pronounced peak is evident at 1 MC. This peak stands as a distinctive signature of ball failure, denoting the defect's interaction with other bearing components during each rotation. Moreover, Fig. 6c manifests a notable peak at the operation cycle of 5, which is indicative of "inner raceway failure". An inner raceway defect leads to a high-frequency impact each time the ball traverses the fault in its revolution, which is prominently represented as a distinct peak in the TSA-spectrum.

Combining the parameters of Bearing 6205, for each turn of the rotating shaft, the cage train (and all rolling elements) moves 0.4 turns. This indicates that with every 2.5 turns of the rotating shaft, all rolling elements complete one full rotation and, with every 5 turns, the rolling elements make two full rotations. As a result, every 5 turns will reset all conditions of both the rotating shaft and rolling elements (and cage train), signifying that the basic cycle is 5 MC. Particularly, we focus on the TSA-spectrum with operation cycles close to 5 MC, as it represents the primary resetting point for bearing elements, making it essential for understanding bearing health.

3.2.2 Fault signal extraction

By exploring the TSA-spectra, we can obtain the precise basic cycle of a given signal. Then, we can directly apply the TSA to the signal with the precise operation cycle and obtain the denoised signal of our interest.

Taking the fourth data sample in Table 1 as an example, the result of TSA is illustrated in Fig. 7a. The shifted raw data is presented in cyan, while the black curve is the TSA vector, namely, the averaged result of the shifted raw data. The operation cycle is 167.171 ms, which is the time required for 5 turns of the rotating shaft. It can be observed that there are 18 obvious pulse-like signals. Considering that there are nine rolling elements of Bearing 6205, the 18 pulse-like signals can be divided into two groups. The first nine pulses, namely, (1)–(9) in Fig. 7a, are the first time the nine rolling elements run across the defect area on the outer race, while the other nine pulses, (1′)–(9′), relate to the second time the rolling elements run across the defect area. Note that the pulses (i) and (i') are actually the signals of the same rolling ball running across the defect area. However, there is a 180° phase difference on the inner race between pulse (i) and (i') (i=1, 2, ⋯, 9), since every 2.5 turns of the rotating shaft lead to a 180° phase change on the inner race.

Let us focus on the waveform of pulse (3). We zoom in on the x-axis as presented in Fig. 7b. It can be observed that the shifted raw data consists of a series of similar waveforms with small phase differences. The smoothing effect V_{SE} is approximately 0.12 ms. This implies that during the application of the TSA process, the smoothing effect of the equivalent moving average filter corresponds to a time window of about 0.12 ms. Specifically, this indicates that short-term fluctuations are averaged and suppressed over this time scale, making the periodic components more prominent. In other words, the instantaneous variations of the signal are smoothed out within this time window, thereby better revealing its periodic characteristics. Particularly, we visualize the shifted raw data in an image style. Fig. 7c shows a periodic change in phase space, at approximately 0.12 ms for every 5 turns of the rotating shaft. The phase changing phenomenon is caused by the unstable rotating speed of the driving motor, which will lead to an additional smoothing effect on the TSA vector.

Additionally, we can estimate the phase differences between every two sampling cycles of the shifted raw data by using a correlation function. Allowing a phase shift operation, we obtain the result of aligned raw data and a corrected TSA vector, as illustrated in Fig. 7d, where the lines in magenta are the aligned raw data within one major cycle. Similarly, as shown in Fig. 7c, we also visualize the aligned raw data in an image style as displayed in Fig. 7e, where the parallel stripes indicate that the variance of rotation speed is

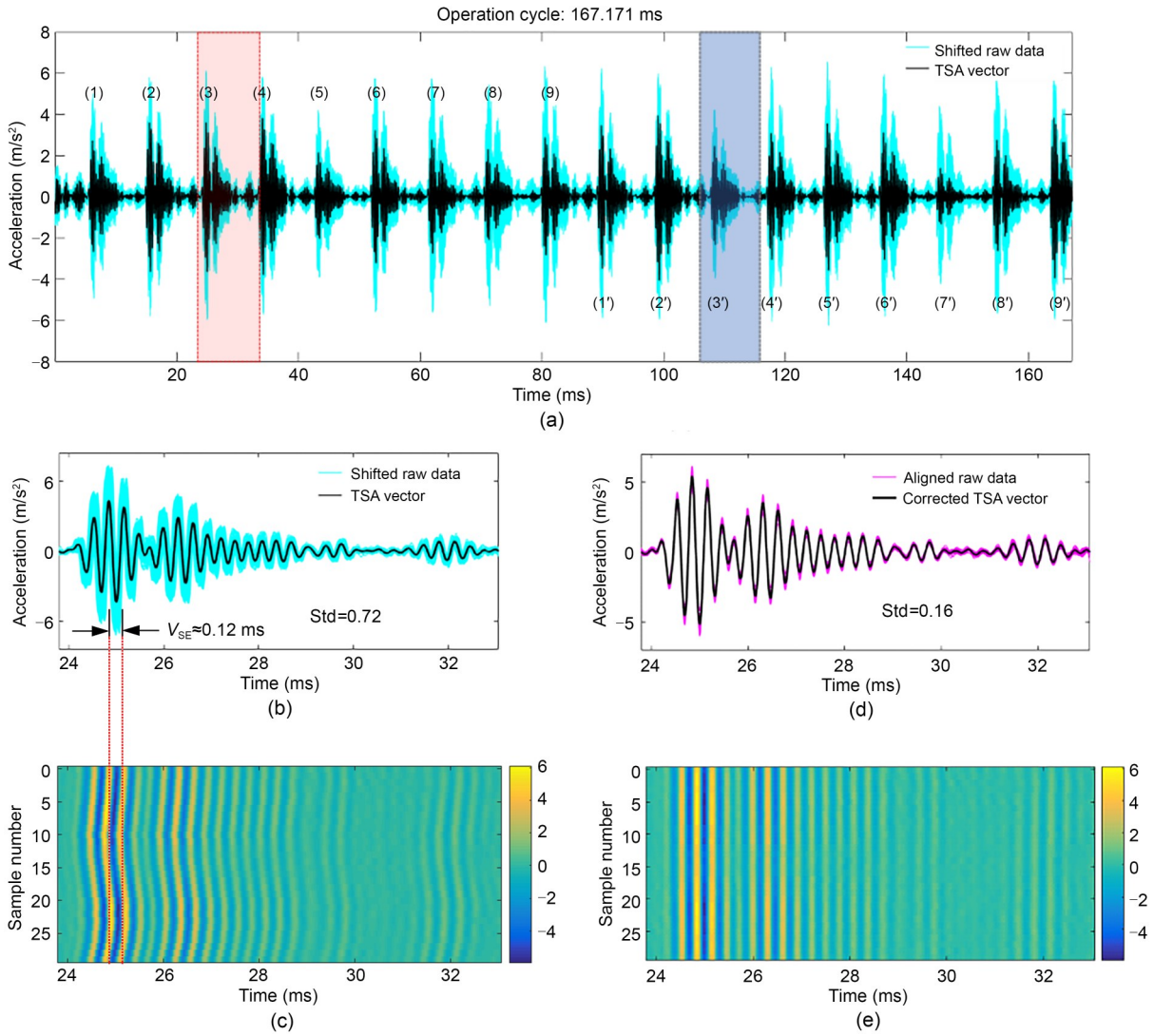

Fig. 7 TAS of Sample 135 with outer raceway failure fault type: (a) TSA result with shifted raw data and TSA vector, showing 18 pulse-like signals from Bearing 6205; (b) zoomed waveform of pulse, highlighting slight phase differences; (c) shifted raw data visualized, indicating periodic phase changes; (d) aligned raw data and corrected TSA vector, reducing rotation speed variance; (e) standard deviation comparison, demonstrating improved waveform consistency

reduced. To address the performance of the alignment process, we calculate the standard deviation of the shifted raw data and aligned raw data with respect to different sample numbers, namely, along the *y*-axis of Figs. 7b and 7d, respectively. The standard deviation (Std) of the aligned raw data is reduced to 0.16 from that of the shifted raw data, which is 0.72. The result in Fig. 7d shows a good repeatability of the acceleration waveform of a rotating bearing.

3.2.3 Extracted fault signal comparison

By applying the TSA method to the four data samples presented in Table 1, we can extract the featured waveform within one entire cycle of each case. The results are presented in Fig. 8. The following points can be drawn from the results in Fig. 8.

1. For a normal bearing without defects, as presented in Figs. 8a and 8b, the TSA vector over the operation cycle of 5 MC is a stationary waveform consisting of two sinusoidal signals with cycles of approximately 2.78 and 0.12 ms, respectively. These two sinusoidal signals relate to the natural vibration period of the test apparatus.

2. In Figs. 8c and 8d, the BF case, the TSA vector contains information on both the rotation of the cage train and the self-rotation of the rolling elements. Each

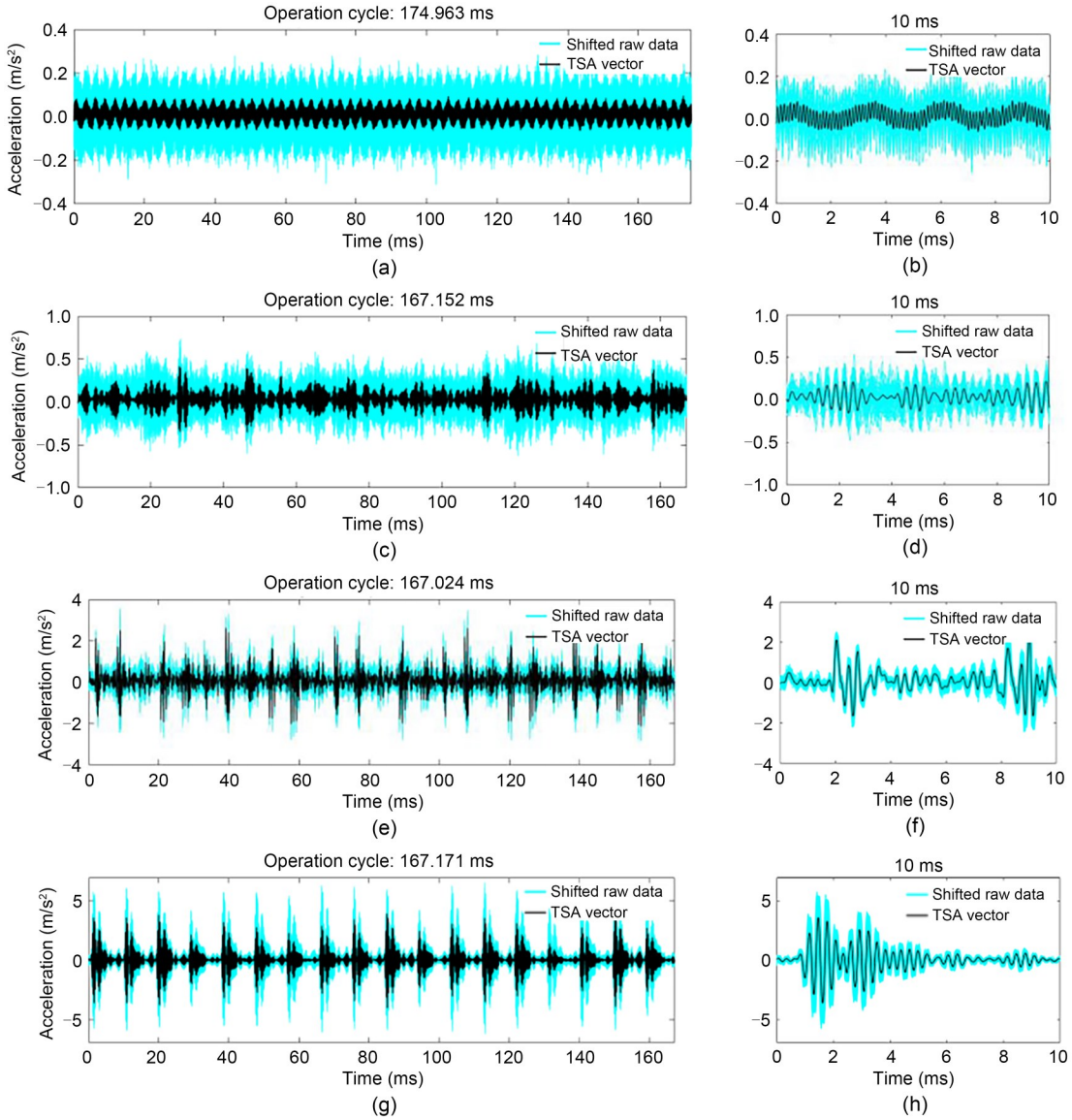

Fig. 8 Extracted waveforms of different fault types: (a), (c), (e), and (g) relate to Files 1 to 4 in Table 1; (b), (d), (f), and (h) are enlarged views of the first 10 ms of the waveform. References to color refer to the online version of this article

hit between the defect area on the rolling elements and the contact point on the inner race or outer race will cause a hitting signal. Since the hitting frequency is higher than the vibration damping speed, different hitting signals overlap together, and it is difficult to find the pattern of a single hit.

3. In Fig. 8e, the IRF case, we can observe approximately 27 pulse-like patterns within the entire cycle. Similarly, in Fig. 8g, the ORF_CE case, there are 18 significant pulse-like patterns. Both fault types are related to the number of rolling elements in the cage train, which is 9 for Bearing 6205. Consequently, we know that within a basic cycle of 5 MC, each ball hits the defect area 3 times for the inner race and 2 times for the outer race.

4 Conclusions

This paper introduced a TSA-spectrum using super-resolution analysis to visualize periodic components in signals. Three propositions were developed and proven to reveal TSA's mathematical properties for quasiperiodic signals. A case study demonstrated TSA's effectiveness in diagnosing bearing faults.

The main findings are summarized as follows:

1. The theoretical framework of TSA, enhanced by super-resolution analysis, effectively analyzes periodic components in quasiperiodic signals.

2. TSA provides more detailed information on cross-effects between periodic components compared to DFT, making it a valuable supplement in the long-period range.

3. The case study showed TSA's superiority in processing vibration signals from defective bearings, illustrating its practical diagnostic benefits.

4. TSA has potential for further exploration in revealing the PAP and its applications in QSP.

In summary, TSA-spectrum and super-resolution analysis significantly enhance the precision and reliability of bearing-fault diagnosis, contributing to improved predictive maintenance and machinery reliability. This study lays the groundwork for more efficient fault diagnosis in bearing health monitoring.

Acknowledgments

This work is supported by the National Natural Science Foundation of China (Nos. 52008198, 51425804, U20A20283, and U1813222), the Shenzhen International Cooperation Research Program (No. GJHZ20200731095009029), the Shenzhen Science and Technology Program (Nos. RCBS20210609103823048 and KJZD20230923114916032), the Foundation of the Department of Science and Technology of Guangdong Province (No. 2019TQ05Z654), and the Guangdong Provincial Key Laboratory of Construction Robotics and Intelligent Construction (No. 2022KSYS013), China.

Author contributions

Wei FENG designed the research. Yuan WANG and Huiyue TANG processed the corresponding data. Zengle REN wrote the first draft of the manuscript. Xin'an CHEN helped to organize the manuscript. Zengle REN revised and edited the final version.

Conflict of interest

Zengle REN, Yuan WANG, Huiyue TANG, Xin'an CHEN, and Wei FENG declare that they have no conflict of interest.

References

Ahamed N, Pandya Y, Parey A, 2014. Spur gear tooth root crack detection using time synchronous averaging under fluctuating speed. *Measurement*, 52:1-11. https://doi.org/10.1016/j.measurement.2014.02.029

Bommert A, Sun XD, Bischl B, et al., 2020. Benchmark for filter methods for feature selection in high-dimensional classification data. *Computational Statistics & Data Analysis*, 143:106839. https://doi.org/10.1016/j.csda.2019.106839

Bravo-Imaz I, Ardakani HD, Liu ZC, et al., 2017. Motor current signature analysis for gearbox condition monitoring under transient speeds using wavelet analysis and dual-level time synchronous averaging. *Mechanical Systems and Signal Processing*, 94:73-84. https://doi.org/10.1016/j.ymssp.2017.02.011

Camerini V, Coppotelli G, Bendisch S, et al., 2019. Impact of pulse time uncertainty on synchronous average: statistical analysis and relevance to rotating machinery diagnosis. *Mechanical Systems and Signal Processing*, 129:308-336. https://doi.org/10.1016/j.ymssp.2019.04.017

CWRU (Case Western Reserve University), 2019. Bearing Data Center: Seeded Fault Test Data. https://engineering.case.edu/bearingdatacenter

Chaumon M, Bishop DV, Busch NA, 2015. A practical guide to the selection of independent components of the electroencephalogram for artifact correction. *Journal of Neuroscience Methods*, 250:47-63. https://doi.org/10.1016/j.jneumeth.2015.02.025

Chen JL, Li ZP, Pan J, et al., 2016. Wavelet transform based on inner product in fault diagnosis of rotating machinery: a review. *Mechanical Systems and Signal Processing*, 70-71:1-35. https://doi.org/10.1016/j.ymssp.2015.08.023

Chen ZG, Zhai WM, Wang KY, 2019. Vibration feature evolution of locomotive with tooth root crack propagation of gear transmission system. *Mechanical Systems and Signal Processing*, 115:29-44. https://doi.org/10.1016/j.ymssp.2018.05.038

Combet F, Gelman L, 2007. An automated methodology for performing time synchronous averaging of a gearbox signal without speed sensor. *Mechanical Systems and Signal Processing*, 21(6):2590-2606. https://doi.org/10.1016/j.ymssp.2006.12.006

de Smidt MR, 2010. Internal Vibration Monitoring of a Planetary Gearbox. MS Thesis, University of Pretoria, Pretoria, South Africa.

Delvecchio S, Bonfiglio P, Pompoli F, 2018. Vibro-acoustic condition monitoring of internal combustion engines: a critical review of existing techniques. *Mechanical Systems and Signal Processing*, 99:661-683. https://doi.org/10.1016/j.ymssp.2017.06.033

Fong S, Harmouche J, Narasimhan S, et al., 2020. Mean shift clustering-based analysis of nonstationary vibration signals for machinery diagnostics. *IEEE Transactions on Instrumentation and Measurement*, 69(7):4056-4066. https://doi.org/10.1109/TIM.2019.2944503

Gabrić D, Aumiler D, Vuletić M, et al., 2021. Thermal evaluation by infrared thermography measurement of osteotomies performed with Er:YAG laser, piezosurgery and surgical drill—an animal study. *Materials*, 14(11):3051. https://doi.org/10.3390/ma14113051

Gao WY, Li H, Zhong MH, et al., 2023. The separate clock drift matched filter to detect time synchronization attacks toward global navigation satellite systems. *IEEE Transactions on Industrial Electronics*, 70(6):6305-6315. https://doi.org/10.1109/TIE.2022.3194578

Gothwal H, Kedawat S, Kumar R, 2011. Cardiac arrhythmias detection in an ECG beat signal using fast Fourier transform and artificial neural network. *Journal of Biomedical Science and Engineering*, 4(4):289-296. https://doi.org/10.4236/jbise.2011.44039

Gupta V, Chopda MD, Pachori RB, 2019. Cross-subject emotion recognition using flexible analytic wavelet transform from EEG signals. *IEEE Sensors Journal*, 19(6): 2266-2274. https://doi.org/10.1109/JSEN.2018.2883497

Halim EB, Choudhury MAAS, Shah SL, et al., 2008. Time domain averaging across all scales: a novel method for detection of gearbox faults. *Mechanical Systems and Signal Processing*, 22(2):261-278. https://doi.org/10.1016/j.ymssp.2007.08.006

Hong M, Wang Q, Su ZQ, et al., 2014. In situ health monitoring for bogie systems of CRH380 train on Beijing-Shanghai high-speed railway. *Mechanical Systems and Signal Processing*, 45(2):378-395. https://doi.org/10.1016/j.ymssp.2013.11.017

Lee J, Wu FJ, Zhao WY, et al., 2014. Prognostics and health management design for rotary machinery systems–reviews, methodology and applications. *Mechanical Systems and Signal Processing*, 42(1-2):314-334. https://doi.org/10.1016/j.ymssp.2013.06.004

Li YF, Liang XH, Lin JH, et al., 2018. Train axle bearing fault detection using a feature selection scheme based multiscale morphological filter. *Mechanical Systems and Signal Processing*, 101:435-448. https://doi.org/10.1016/j.ymssp.2017.09.007

Lin CC, Hu WC, Chen CM, et al., 2008. Heart rate detection in highly noisy handgrip electrocardiogram. 2008 Computers in Cardiology, IEEE, p.477-480.

Lin T, Chen G, Ouyang WL, et al., 2018. Hyper-spherical distance discrimination: a novel data description method for aero-engine rolling bearing fault detection. *Mechanical Systems and Signal Processing*, 109:330-351. https://doi.org/10.1016/j.ymssp.2018.01.009

Ma JM, Tao R, 2021. Research progress of the sampling theorem associated with the fractional Fourier transform. *Journal of Beijing Institute of Technology*, 30(3):195-204. https://doi.org/10.15918/j.jbit1004-0579.2021.041

Ma M, Sun C, Zhang C, et al., 2019. Subspace-based MVE for performance degradation assessment of aero-engine bearings with multimodal features. *Mechanical Systems and Signal Processing*, 124:298-312. https://doi.org/10.1016/j.ymssp.2018.12.008

Mannan MMN, Kamran MA, Kang S, et al., 2018. Effect of EOG signal filtering on the removal of ocular artifacts and EEG-based brain–computer interface: a comprehensive study. *Complexity*, 2018(1):4853741. https://doi.org/10.1155/2018/4853741

Martens P, Verbrugge FH, Bertrand PB, et al., 2018. Effect of cardiac resynchronization therapy on exercise-induced pulmonary hypertension and right ventricular-arterial coupling: a cardiopulmonary exercise testing imaging evaluation. *Circulation: Cardiovascular Imaging*, 11(9):e007813. https://doi.org/10.1161/CIRCIMAGING.118.007813

McFadden PD, 1987. A revised model for the extraction of periodic waveforms by time domain averaging. *Mechanical Systems and Signal Processing*, 1(1):83-95. https://doi.org/10.1016/0888-3270(87)90085-9

McFadden PD, 1989. Interpolation techniques for time domain averaging of gear vibration. *Mechanical Systems and Signal Processing*, 3(1):87-97. https://doi.org/10.1016/0888-3270(89)90024-1

McFadden PD, Toozhy MM, 2000. Application of synchronous averaging to vibration monitoring of rolling element bearings. *Mechanical Systems and Signal Processing*, 14(6):891-906. https://doi.org/10.1006/mssp.2000.1290

Mishra C, Samantaray AK, Chakraborty G, 2016. Rolling element bearing defect diagnosis under variable speed operation through angle synchronous averaging of wavelet de-noised estimate. *Mechanical Systems and Signal Processing*, 72-73:206-222. https://doi.org/10.1016/j.ymssp.2015.10.019

Nagwanshi N, Potnis A, 2023. Detection of Epilepsy patients using coot optimization based feed forward multilayer neural network. *Journal of Experimental & Theoretical Artificial Intelligence*, 1-26. https://doi.org/10.1080/0952813X.2023.2256739

Peng DD, Liu ZL, Wang H, et al., 2019. A novel deeper one-dimensional CNN with residual learning for fault diagnosis of wheelset bearings in high-speed trains. *IEEE Access*, 7:10278-10293. https://doi.org/10.1109/ACCESS.2018.2888842

Pitarresi G, Cappello R, Catalanotti G, 2020. Quantitative thermoelastic stress analysis by means of low-cost setups. *Optics and Lasers in Engineering*, 134:106158. https://doi.org/10.1016/j.optlaseng.2020.106158

Qiao W, Lu DG, 2015. A survey on wind turbine condition monitoring and fault diagnosis—part II: signals and signal processing methods. *IEEE Transactions on Industrial Electronics*, 62(10):6546-6557. https://doi.org/10.1109/TIE.2015.2422394

Rahman AGA, Chao OZ, Ismail Z, 2011. Effectiveness of impact-synchronous time averaging in determination of dynamic characteristics of a rotor dynamic system. *Measurement*, 44(1):34-45. https://doi.org/10.1016/j.measurement.2010.09.005

Randall RB, Antoni J, 2011. Rolling element bearing diagnostics—a tutorial. *Mechanical Systems and Signal Processing*, 25(2): 485-520. https://doi.org/10.1016/j.ymssp.2010.07.017

Roth M, Hendeby G, Fritsche C, et al., 2017. The ensemble Kalman filter: a signal processing perspective. *EURASIP Journal on Advances in Signal Processing*, 2017(1):56. https://doi.org/10.1186/s13634-017-0492-x

Roy SK, Mohanty AR, Kumar CS, 2016. Fault detection in a multistage gearbox by time synchronous averaging of the instantaneous angular speed. *Journal of Vibration and Control*, 22(2):468-480. https://doi.org/10.1177/1077546314533582

Salameh JP, Cauet S, Etien E, et al., 2018. Gearbox condition monitoring in wind turbines: a review. *Mechanical Systems*

and Signal Processing, 111:251-264. https://doi.org/10.1016/j.ymssp.2018.03.052

Schmidt S, Zimroz R, Heyns PS, 2021. Enhancing gearbox vibration signals under time-varying operating conditions by combining a whitening procedure and a synchronous processing method. *Mechanical Systems and Signal Processing*, 156:107668. https://doi.org/10.1016/j.ymssp.2021.107668

Sim J, Min JH, Kim D, et al., 2022. A python based tutorial on prognostics and health management using vibration signal: signal processing, feature extraction and feature selection. *Journal of Mechanical Science and Technology*, 36(8):4083-4097. https://doi.org/10.1007/s12206-022-0728-z

Smith WA, Randall RB, 2015. Rolling element bearing diagnostics using the Case Western Reserve University data: a benchmark study. *Mechanical Systems and Signal Processing*, 64-65:100-131. https://doi.org/10.1016/j.ymssp.2015.04.021

Sugavanam S, Kopae MK, Peng JS, et al., 2019. Analysis of laser radiation using the nonlinear Fourier transform. *Nature Communications*, 10(1):5663. https://doi.org/10.1038/s41467-019-13265-4

Sun RB, Yang ZB, Chen XF, et al., 2018. Gear fault diagnosis based on the structured sparsity time-frequency analysis. *Mechanical Systems and Signal Processing*, 102:346-363. https://doi.org/10.1016/j.ymssp.2017.09.028

Syed SH, Muralidharan V, 2022. Feature extraction using Discrete Wavelet Transform for fault classification of planetary gearbox–a comparative study. *Applied Acoustics*, 188:108572. https://doi.org/10.1016/j.apacoust.2021.108572

Talhaoui H, Menacer A, Kessal A, et al., 2014. Fast Fourier and discrete wavelet transforms applied to sensorless vector control induction motor for rotor bar faults diagnosis. *ISA Transactions*, 53(5):1639-1649. https://doi.org/10.1016/j.isatra.2014.06.003

Tan WZ, Wu JM, Ni D, et al., 2021. Dynamic modeling and simulation of double-planetary gearbox based on bond graph. *Mathematical Problems in Engineering*, 2021:3964808. https://doi.org/10.1155/2021/3964808

Teng W, Ding X, Zhang YY, et al., 2017. Application of cyclic coherence function to bearing fault detection in a wind turbine generator under electromagnetic vibration. *Mechanical Systems and Signal Processing*, 87:279-293. https://doi.org/10.1016/j.ymssp.2016.10.026

Thakor NV, Tong S, 2004. Advances in quantitative electroencephalogram analysis methods. *Annual Review of Biomedical Engineering*, 6:453-495. https://doi.org/10.1146/annurev.bioeng.5.040202.121601

Thibault É, Désilets FL, Poulin B, et al., 2023. Comparison of signal processing methods considering their optimal parameters using synthetic signals in a heat exchanger network simulation. *Computers & Chemical Engineering*, 178:108380. https://doi.org/10.1016/j.compchemeng.2023.108380

Tian CW, Zheng MH, Zuo WM, et al., 2023. Multi-stage image denoising with the wavelet transform. *Pattern Recognition*, 134:109050. https://doi.org/10.1016/j.patcog.2022.109050

Touret T, Changenet C, Ville F, et al., 2018. On the use of temperature for online condition monitoring of geared systems–a review. *Mechanical Systems and Signal Processing*, 101:197-210. https://doi.org/10.1016/j.ymssp.2017.07.044

Wang D, Tsui KL, Miao Q, 2018a. Prognostics and health management: a review of vibration based bearing and gear health indicators. *IEEE Access*, 6:665-676. https://doi.org/10.1109/ACCESS.2017.2774261

Wang D, Zhao Y, Yi C, et al., 2018b. Sparsity guided empirical wavelet transform for fault diagnosis of rolling element bearings. *Mechanical Systems and Signal Processing*, 101:292-308. https://doi.org/10.1016/j.ymssp.2017.08.038

Wang TY, Liang M, Li JY, et al., 2014. Rolling element bearing fault diagnosis via fault characteristic order (FCO) analysis. *Mechanical Systems and Signal Processing*, 45(1):139-153. https://doi.org/10.1016/j.ymssp.2013.11.011

Wang TY, Han QK, Chu FL, et al., 2019. Vibration based condition monitoring and fault diagnosis of wind turbine planetary gearbox: a review. *Mechanical Systems and Signal Processing*, 126:662-685. https://doi.org/10.1016/j.ymssp.2019.02.051

Wang X, Liu CW, Bi FR, et al., 2013. Fault diagnosis of diesel engine based on adaptive wavelet packets and EEMD-fractal dimension. *Mechanical Systems and Signal Processing*, 41(1-2):581-597. https://doi.org/10.1016/j.ymssp.2013.07.009

Wang XY, Li YW, Gao HX, et al., 2023. A causal intervention scheme for semantic segmentation of quasi-periodic cardiovascular signals. *IEEE Journal of Biomedical and Health Informatics*, 27(7):3175-3186. https://doi.org/10.1109/JBHI.2023.3270978

Yao RH, Jiang HK, Li XQ, et al., 2022. Bearing incipient fault feature extraction using adaptive period matching enhanced sparse representation. *Mechanical Systems and Signal Processing*, 166:108467. https://doi.org/10.1016/j.ymssp.2021.108467

Zhang L, Hu N, 2019. Time domain synchronous moving average and its application to gear fault detection. *IEEE Access*, 7:93035-93048. https://doi.org/10.1109/ACCESS.2019.2927762

Zhang ZZ, Li SM, Wang JR, et al., 2019. General normalized sparse filtering: a novel unsupervised learning method for rotating machinery fault diagnosis. *Mechanical Systems and Signal Processing*, 124:596-612. https://doi.org/10.1016/j.ymssp.2019.02.006

Zhao Y, Zhao H, Ai J, et al., 2022. Robust data-driven fault detection: an application to aircraft air data sensors. *International Journal of Aerospace Engineering*, 2022(1):2918458. https://doi.org/10.1155/2022/2918458

Electronic supplementary materials

Section S1